Intra-skeletal vascular density in a bipedal hopping macropod with implications for analyses of rib histology

Full title

Intra-skeletal vascular density in a bipedal hopping macropod with implications for analyses of rib histology.

Running title

Rib vascular canal density and intra-skeletal biomechanics

Authors

Tahlia J. Stewart[1*], Julien Louys[2], Justyna J. Miszkiewicz[1]

Affiliations

[1]Skeletal Biology and Forensic Anthropology Research Group, School of Archaeology and Anthropology, Australian National University, Canberra 2601, Australia

[2]Australian Research Centre for Human Evolution, Environmental Futures Research Institute, Griffith University, Brisbane

***Corresponding author**

Tahlia J. Stewart
Skeletal Biology and Forensic Anthropology Research Group
School of Archaeology & Anthropology
The Australian National University
Room 201A, Banks Building
44 Linnaeus Way
Acton, ACT, Australia 2601
Email: Tahlia.Stewart@anu.edu.au
Phone: +61 261 250 256

Abstract

Human ribs are thought to be less affected by mechanical strain at the microscopic level than limb bones, implying that rib remodeling better reflects bone physiological homeostasis. Here, we test the hypothesis that rib tissue will be well vascularized and thus enhance susceptibility to metabolic influence. An intra-skeletal comparison of bone vascular canal density was conducted using a macropod animal model adapted to bipedal habitual hopping. The right humerus, ulna, radius, femur, tibia, fibula, a mid-thoracic and upper-thoracic rib of an eastern grey kangaroo (*Macropus giganteus*) were sectioned at the midshaft, from which histological sections were prepared. Bone vascularity from a maximum of 12 mm^2 of sub-periosteal parallel-fibred and lamellar bone was recorded, resulting in a total of 2,047 counted vessels. Vascular canal density data were corrected by cortical width, maximum length, and midshaft circumference robusticity indices computed for each bone. The fibula consistently had the highest vascular canal density, even when corrected for maximum length, cortical width and midshaft circumference robusticities. This was followed by the mid- and upper-thoracic ribs. Vascularity differences between bones were relatively consistent whether vascular canal density was controlled for by cortical width or midshaft circumference robusticities. Vascular canal density and robusticity indices were also positively and negatively correlated ($p < 0.05$). Results confirm that the ribs are well vascularized, which facilitates bone metabolic processes such as remodeling, but the fibula also appears to be a well vascularized bone. Future research investigating human bone metabolism will benefit from examining thoracic rib or fibula samples.

Keywords: Bone and Bones; Histology; Physiology; Movement

INTRODUCTION

Human ribs are thought to represent exemplar bones to investigate systemic skeletal metabolism that may relate to calcium homeostasis or the influences of diet (Agnew and Stout 2012; Crowder and Rosella 2007; Dominguez and Agnew 2016; Kondo et al. 2000; Paine and Brenton 2006; Tommerup et al. 1993). This is due to their less variable, low-strain remodeling compared to the lower limbs (Skedros et al. 2013). For example, remodeling in the human femur can be initiated by a combination of mechanical loadings that arise from behavior and upper body weight (e.g. tension and compression) (Pfeiffer et al. 2006; also see Skedros et al. 2013 for discussion). On the contrary, most biomechanical loading sustained by the rib is consistent and cyclical in nature, as breathing movements are similar between adult individuals, including elastic bending that occurs with lung cavity expansion and respiratory muscle activation (Agnew and Stout 2012; Kondo et al. 2000). While midthoracic ribs have their own costal cartilage, they are biomechanically and morphologically similar between individuals, as they are constrained by the anatomical environment of the surrounding intercostal muscles and vertebrae (Crowder and Rosella 2007).

The above rationale has formed the basis from which to investigate human skeletal biology in archaeological and modern contexts (e.g. Cox and Sealy 1997; Hedges et al. 2007; Lamb et al. 2014; Mulhern 2000; Pfeiffer et al. 2006; Robling and Stout 2003; Skedros et al. 2013), with some studies incorporating bones other than just the femur and the rib for comparison (e.g. Eleazer & Jankauskas 2016; Fahy et al. 2017). However, not entirely consistent conclusions regarding the rib being a less mechanically impacted bone have been drawn in the literature. For example, using human archeological and historical samples, Pfeiffer et al. (2006) reported inconsistent and highly variable rib vs. femur histomorphometric relationships that did not follow metabolic and biomechanical predictions. Eleazer and Jankauskas (2016) surmised that chronic stress appeared to interrupt relationships between porosity and biomechanical loading in archaeological human ribs, humerii and femora, with ribs having the lowest amount of porosity and femora having the largest. Skedros et al. (2013) collated secondary osteon size and bone volume data for the rib and various lower limb bones (femora, metatarsals, calcanei, radii, humeri, metacarpals) from a range of human and non-human animals including deer (O. *hemionus*, *O. virginianus*), sheep (*O. aries)*, elk (*C. elaphus)*, and black bear (*U. americanus)* (see Table 1 in Skedros et al. 2013 for full details of specimens), to find that bone histological markers and

volume did not consistently follow the expectation that metabolic homeostasis is preferentially maintained at the rib. However, rib tissue in the macaque (*Macaca fascicularis*), when compared against the femur, tibia, and fibula (Lad et al. 2019); and in archeological human remains when contrasted against femur, tibia, humerus, metacarpal, occipital bone, pelvis, clavicle, radius, and thoracic vertebrae samples (Fahy et al. 2017), did show microscopic evidence for high remodeling trends intra-skeletally. To the best of our knowledge, no studies have yet used histology to evaluate rib vascularity intra-skeletally in a macropod model adapted to habitual bipedal hopping. Therefore, our study aimed to build upon prior investigations into the rib being a highly metabolic tissue, adding new kangaroo bone data and insights into bone vascularity.

Predictions and hypotheses

As outlined in the Utah Paradigm of Skeletal Physiology (Frost 2000), bone that is subject to dynamic and repetitive biomechanical load 'regulates' its tissue amount and competence by adapting to strain. This is typically achieved through modeling and/or remodeling and is a complex process dependent on one's minimum effective strain (MES) and other environmental factors (see Hart et al. 2017). Generally, (healthy) limb bone that needs to withstand habitual load will be denser and of a larger cross-sectional area that shows relatively thicker cortices (Frost 1964; Lieberman and Polk 2004). As per the beam theory, new bone tissue deposited in response to strain that exceeds the MES typically forms on the sub-periosteal surfaces of a long bone (Rubin and Lanyon 1987; Robling et al. 2006). This also means that, intra-skeletally, different bones have different rates of remodeling (Fahy et al. 2017; Lad et al. 2019). Inter-skeletally, different locomotor behaviours will also result in a spectrum of remodeling. This was demonstrated in a series of primate species where bipedalism was associated with the highest occurrence of remodeled osteonal bone, as opposed to arboreal quadrupedalism, which had the lowest experiences of bone remodeling (Schaffler and Burr 1984).

If higher rates of remodeling result in increased densities of secondary osteons, then bone vascular canals should also be denser in bone that is consistently metabolically active. Limb bones which are more mechanically strained relative to the rib should accommodate load through increased lamellar space, with fewer vessel types such as Haversian and primary canals. Although this relationship is not simplistic, and complicated by micro-crack repair and dependent on load magnitude. As the ribs are assumed to experience increased

remodeling, a hypothesis that they are also relatively more 'vascular' than other bones can be proposed on the basis that they receive more regular blood supply as a means of nutrients and oxygen transport (Frost 1969; Marenzana and Arnett 2013), and that is also involved in the regulation of calcium homeostasis required for bone health and strength (Lafage-Proust et al. 2015; Peterson and Riggs, 2010). Therefore, bone vascularity, unless studied experimentally (e.g. through fluorescent labelling of samples extracted from animal models subjected to biomechanical experimentation), can be a reflection of biomechanically stimulated remodeling (Robling et al., 2006) and/or stochastic remodeling which is non-targeted and is part of bone maintenance (Eriksen, 2010). Here, we test this hypothesis by measuring bone tissue vascular canal density (number of vessels per mm^2) of the long bones and two ribs in an eastern grey kangaroo (*Macropus giganteus*) which serves as an animal model of intra-skeletal adaptation to two forms of locomotion; bipedal and pentapedal (O'Connor et al. 2014) (Fig. 1).

MATERIALS AND METHODS

Macropus giganteus skeletal samples

A skeleton of an eastern grey kangaroo (*M. giganteus*) was recovered as a subfossil surface find in the Manning Karst Region of eastern New South Wales during part of a paleontological investigation (Price et al. 2019). No animal was sacrificed or harmed in this study, and permissions to excavate were obtained from the landowner. The skull associated with these remains is registered under AODF0927 at the Australian Age of Dinosaurs Museum, Winton, Queensland. Samples from the post-cranial bones have been accessioned into the Hard Tissue Histology collection of thin sections at the Australian National University (ANU accession IDs: ANU SOAA KH18, KU18, KUR18, KLR18, KF18, KR18, KT18, KFEM18). The examined elements were right humerus, ulna, radius, femur, tibia, fibula, a 'mid-thoracic' rib and 'upper-thoracic' rib (Fig. 1, 2). The rib numbers could not be determined, so they were labelled on the basis of their location within the rib cage.

In addition to *M. giganteus*, three other species of kangaroos are currently recognized as large kangaroos: *Osphranter rufus* (red), *M. fuliginosus* (western grey), and *Osphranter antilopinus* (antilopine) (Celik et al. 2019). Kangaroo research has dealt with taphonomic questions such as post-mortem disarticulation in Australian environments (Reed 2001); genomic sequencing elucidating marsupial evolution (Celik et al.

2019; Nilsson et al. 2010; Prideaux and Warburton 2010); reproduction and growth observations in captive and wild groups with a focus on sex ratios, sexual maturity, birthing and mortality, sociality, diet, ecology (Poole 1976; Russell 1974); and anatomical descriptions and behavioral observations that have provided insights into movement and sexual dimorphism of the musculature (e.g. Alexander and Vernon 1975; Coulson 2010; Dawson 1995; Flannery 1982; Richardson 2012; Szalay 1994, Warburton et al. 2013).

Kangaroo movement has been well studied to establish their locomotion through bipedal hopping, and the important role of the tail in pentapedal locomotion and hopping (Alexander & Vernon 1975; Dawson 1995; Dawson et al. 2015; 2014; McGowan et al. 2008; O'Connor et al. 2014). Kangaroos have robust but reduced specialized forelimbs (Harvey and Warburton 2010) (Fig. 1). They are used during locomotion on the ground to support the body during pentapedal movement, aided by the tail, as hindlimbs are protracted; and during feeding, manipulation activities, and grooming (Harvey and Warburton 2010; Warburton et al. 2013). Forelimbs are also specialized in that their morphology needs to facilitate a joey's ability to climb out of the mother's pouch (Cooper and Steppan 2010). The tail is often referred to as the 'fifth limb' which assists with the slow gait of kangaroos (Dawson et al. 2015). The hindlimbs are relatively large with a robust femur relative to the tibia and fibula that experience weight-bearing and mechanical stimulation from hopping (Fig. 1, Dawson et al. 2015). However, the tibia and fibula are particularly elongated and relatively gracile where mechanical and physiological properties are optimized as an adaptation to kangaroo locomotion (Dawson et al. 2015). This ensures efficiency during low speed pentapedal locomotion and high speed bipedal hopping (Dawson et al. 2014). The femorotibial articulation receives principal loadbearing, but a rotation torque is prevented due to a specialized knee complex (Miller et al. 2017). The (distal) tibia receives predominantly bending and some axial load (Alexander and Vernon 1975).

Limited prior histology records are available for any large kangaroo species. Soft tissue histology has been described for the fibular meniscus (Miller et al. 2017) and used in other tissue analyses such spermatogenesis in sections from testes (Poole 1976). Femur and humerus bone histology has been described for *M. fuliginosus* in relation to ontogeny and the development of fibrocartilage entheses (Chinsamy and Warburton 2021). Our case study was also preliminarily presented at the 2019 International Symposium on

148 Paleohistology in Cape Town, South Africa (Stewart et al. 2019). Because our study was designed with
149 anthropological questions in mind, we emphasize that it focuses on localized vascularization of midshaft bones
150 only and thus invites future qualitative examination and description of *M. giganteus* bone tissue matrices in
151 relation to life history traits.

152 **Osteological and histological procedures**

153 Prior to histology preparation, all bones were measured for midshaft circumference and length (e.g.
154 Croker et al. 2016; Table 1). They were then sectioned transversely at the midshaft (Fig. 2), which was defined
155 as the midpoint of the maximum length. Rib maximum length was measured following bone curvature, but
156 other bones were measured using an osteometric board. The femur and tibia were sectioned using an Eclipse®
157 20T handsaw fitted with a Starrett ® SF1232 HSS 32T 12"/300 mm blade. Other bones were sectioned with a
158 handheld Arlec® Supertool fitted with Dremel® blades. Sections removed were approximately 1 cm thick.
159 Histological preparation of bone was conducted in the Histology lab of the ANU School of Archaeology and
160 Anthropology, following standard methods (e.g. Miszkiewicz et al. 2019; 2020). Sections were embedded in
161 Buehler EpoxiCure® epoxy resin, before being reduced to approximately 0.5 cm, using a Kemet Micracut®
162 151 precision cutter fitted with a 150 mm diamond blade. Embedded samples were dried and affixed to glass
163 slides with Araldite®. Sections were further reduced to a thickness of approximately 100 µm using a Buehler®
164 EcoMet 300 grinder-polisher, first with Buehler abrasive paper and then a Buehler polishing cloth. Slides were
165 then given an ultrasonic bath, dehydrated and cleared as per methodological standards (Mendelow and Hamilton
166 1950; Williams 1994).

167 Slides were imaged using an Olympus BX53 high powered microscope and a DP74 camera, with
168 cellSens® Olympus 2018 software under transmitted and lambda plate compensated (Olympus U-TP530)
169 polarized light (e.g. Walker et al. 2020). Due to the large size of the tibial and femoral cross-sections (Fig. 2),
170 to keep sampling methodologies consistent, and to target sub-periosteal regions of long bones as per mechanical
171 adaptation principles outlined earlier, we implemented regions of interest (ROIs) for histological analysis. In
172 some prior human bone histology studies it has been suggested that implementing ROIs can accurately represent
173 up to 95% of overall histological variability intra-section (Iwaniec et al. 1998; Villa and Lynnerup 2010). This

has not yet been determined for marsupial bone sections. However, our implementation of ROIs should minimize the effect of intra-section histological variability (e.g. changes in bone matrices and associated vascularity regulated through ontogeny, see Chinsamy and Warburton, 2021) due to, for example, endosteal expansion and periosteal apposition reflecting relatively different growth rates on the respective bone envelopes (van Der Meulen et al. 1993). First, entire captures of the cross-sections were taken to assist with ROI selection and mapping. Using ImageJ® vol. 1.52 software, cross-sections were rotated to the anatomical position and crosshairs overlaid (Fig. 3). Twelve 1 mm^2 ROIs were selected from each cross-section, with three from each of the cranial/anterior, caudal/posterior, medial and lateral sub-periosteal/outer cortical bone (Fig. 3). The mid-point of the outer section border was where the first ROI, located 'underneath' (within ~1 mm depth depending on the preservation of the histology) the periosteal border, was placed. The other two ROIs were then placed on either side of the central ROI, within ~1 mm distance sideways, following diagonal cross-hairs at ~11° (Fig. 3). Exceptions to this were the fibula, whereby 0.5 mm^2 ROIs were selected due to the smaller overall cross-section size (Fig. 2), and the humerus where only nine ROIs were suitably preserved for analysis. Overall, this procedure resulted in vessel data captured from a maximum of 12 mm^2 and minimum of 6 mm^2 areas of bone across the study. The ROIs were imaged at 10x magnification.

Using the ImageJ® vol. 1.52 "multi-point" tool, intact longitudinal vascular canals were counted to obtain density per mm^2, referred to here as vascular canal density (Ca.Dn) (Table 1, Fig. 2, 3, 4; e.g. Shea et al. 2002; Wu et al. 2019). Bone tissue vascular canal density characterizes bone physiology and growth. In mammal cortical bone, four vessel types are usually seen, including primary canals that can be longitudinal, radial, circular, and oblique (Francillon-Vieillot et al. 1990). They are further categorized as primary vessels, or primary and secondary osteons depending on the developmental and remodeling stage of the bone/animal (Huttenlocker et al. 2013). Because we did not examine the thin sections in their entirety, measures of cortical porosity, defined as area or percentage based measures, were not considered because they can also include porous structures which are not blood vessels (Cooper et al. 2016; Dempster et al. 2013). Because we were interested in mostly regional (sub-periosteal or outer cortical segment of bone) blood supply, we used a point count technique to investigate vessel 'occurrence' from which we estimated density per mm^2 (e.g. Prisby 2017; Shea et al. 2002; Wu et al. 2019; Viboolvorakul et al. 2009). We targeted vessels that were longitudinal (i.e.

oriented along the long bone axis) (Fig. 4), because radial vascularity was not consistently observed in all the ROIs. Including radial vessels might have also 'duplicated' the count of neighboring longitudinal vessels and introduced a new variable of 'connectivity' (Cooper et al. 2003), though we do acknowledge that bone vascular orientation is of importance when examining bone biomechanics (Britz et al. 2012). Included in our analyses were: simple primary vessels scattered across parallel-fibered bone, as well as occasional primary and secondary osteon structures seen in lamellar bone (see Ziv et al. 1996). These were counted if they were rounded, complete and were wholly captured within the ROI. Those that were cut off by the ROI image border were not counted (Table 1). Because of the combination of these vessel types seen in our ROIs, we can deduce that they had formed as a result of both ontogenetic modeling and remodeling processes acting on the bones. At least 95 blood vessels were counted per bone, totaling 2,047 for the individual. Fibula raw vascular canal density was doubled to account for the halved ROI size.

Because of the intra-skeletal variability in bone size (Fig. 1, 2), we computed robusticity indices (RIs) based on cortical width (Ct.Wi), midshaft circumference (Circ) and maximum bone length (Max.Length) (Table 1). These follow common practices that divide the midshaft size by bone length in various mammals (e.g. Elissamburu and Vizcaino 2004; Vizcaíno and Milne 2002). Cortical width was measured in ImageJ® vol. 1.52 (using the "straight line" tool), with 12 measurements taken per bone cross-section at the corresponding outer axis for each ROI (Fig. 3a).

Statistical procedures

We checked for intra-observer and inter-observer relationships between vessel counts from 19 images (>20% of data), which were randomly selected using a random number generator. For the intra-observer comparison, TJS re-counted the images 23 months after the first analysis. A week later, another co-author of the study (JJM), conducted vessel counts from the same images separately. Because of the small sample size, the level of relationship between the duplicated data was evaluated using the coefficient value of a Spearman's *Rho* Rank test, with $Rho > 0.9$ and $p < 0.05$ indicating a strong relationship between the ranks (Taylor, 1980). As this is a case study, we comment on trends in the descriptive data first. Total vascular canal density (Tt.Ca.Dn) (Table 1) was calculated for each bone by summing raw counts to assess differences between bones prior to

correcting by the robusticity indices (Ct.Wi.RIs, Circ.RIs). The Ca.Dn counts for each ROI were then corrected by the robusticity indices (Ct.Wi.RIs, Circ.RIs) to help account for inequalities in bone size vs. tissue areas sampled in the study. Second, non-parametric Spearman's *rho* correlations were conducted to check for positive or negative relationships between Tt.Ca.Dn and Circ.RIs, and corrected Ca.Dn for each ROI with their respective Ct.Wi.RIs. A related samples Friedman's two-way analysis of variance of ranks (pairwise comparison) was also performed to assess whether statistically significant vascularity data distribution varies between different bones.

RESULTS

The evaluation of replicated data resulted in strong positive correlations for the intra ($Rho = 0.991$, $p = <0.0001$), and inter-observer ranks ($Rho = 0.982$, $p = <0.0001$). We deemed the data suitable for analysis and interpretation in this study.

Do ribs have a higher vascular canal density than the other bones?

Descriptive statistics indicate that the fibula was, on average, the most densely vascular skeletal element, followed by the upper- and mid-thoracic rib (Fig. 5a, Table 2). The humerus was the least densely vascular bone, followed by the femur (Fig. 5a). The fibula remained the most densely vascular after controlling for Circ.RIs, followed by the mid- and upper- thoracic rib (**Fig. 5b**). When corrected Ca.Dn was examined per Ct.Wi.RI, the ulna appeared more densely vascular than the radius, but the fibula remained the most densely vascular bone, followed by the mid- and upper- thoracic ribs (Fig. 5c). Whether controlled for by Circ.RI or Ct.Wi.RI, the fibula, the mid- and upper- thoracic ribs remained the bones with the three highest corrected Ca.Dn values (Fig. 5b, 5c).

Do vascular canal densities correlate with robusticity indices intra-skeletally?

As the humerus had fewer ROIs than the other bones, it was excluded from any analysis involving Tt.Ca.Dn, which was a sum of recorded Ca.Dn (Table 1). There was a significant negative relationship between corrected Tt.Ca.Dn and Circ.RI ($rho = -0.821$, $p = 0.023$) (Fig. 5d). A negative relationship between corrected Ca.Dn and Ct.Wi.RI was also identified ($rho = -0.535$, $p < 0.0001$) (Fig. 5e). When sub-divided by bone (Table

252 3), we identified strong positive relationships between Ca.Dn and Ct.WI.RI in the radius (*rho* = 0.773, *p* =
253 0.003) and thoracic rib (*rho* = 0.633, *p* = 0.027), but a negative correlation in the tibia (*rho* = -0.636, *p* = 0.026)
254 (Table 3).

255 Results of the Friedman's pairwise comparison indicate that corrected Ca.Dn was statistically
256 significantly different between most bones (Friedman's Q = 42.168, *p* = <0.0001); Fig. 5f). Statistically
257 significant differences were identified in several bone pairs, further separating those most densely vascular
258 elements (the ribs and fibula) from the other elements, particularly those least densely vascular (humerus and
259 femur).

260 **DISCUSSION**

261 While both the upper- and mid-thoracic ribs had increased vascular density compared to the weight-
262 bearing bones, the thoracic rib proved to be the most consistently highly vascular rib. This confirms that middle
263 ribs are the most appropriate bones for assessments that exclude the effect of mechanical loading on bone tissue
264 microstructure, as proposed in prior anthropological literature (e.g. Crowder and Rosella 2007; Dominguez and
265 Agnew 2016).

266 Our results suggest that the rib possibly receives relatively substantial blood supply, which agrees with
267 suggestions elsewhere that it best reflects systemic metabolism and a higher remodeling rate (Frost 1969). The
268 consistent and cyclical load a rib experiences is less variable in nature than seen in other bones. Dominguez and
269 Agnew (2016) suggested that respiration evokes predominantly tension on the cutaneous rib cortex, and
270 compression in the plural rib cortex. Comparing the kangaroo patterns of biomechanical demands to those seen
271 in humans (Fatima et al. 2019), the relatively high vascularity of the rib can be used as evidence that indeed the
272 rib is metabolically more sensitive than the other bones considered in our study. However, this is not to say that
273 the biomechanical loading of the rib is negligent. In prior studies of similar study design to ours, albeit
274 conducted on the macaque (*Macaca fascicularis*) (Lad et al. 2019), cortical porosity of the rib correlated with
275 mechanical load frequency, when compared to other elements of the appendicular skeleton. This interpretation
276 is alternate to ours of physiological metabolism, whereby Lad et al. (2019) proposed that microcrack generation
277 as a result of respiratory movements can increase remodeling to target localized damaged bone tissue. This

raises important comparative and alternative interpretations for future research on larger samples, where experiments should also include rib load frequency in histological examination.

We also found the fibula was highly vascular, seemingly even more so than the middle ribs. In human cadavers, the fibula was previously identified as a biomechanically relevant bone, though it is less impacted by weight-bearing than other lower leg bones (Goh et al. 1992; Takebe et al. 1984). Ankle movement examination in such human cases reported that the largest loads occur with full dorsiflexion and eversion (Goh et al. 1992; Takebe et al. 1984). These experiments somewhat mirror our kangaroo fibula histology finding whereby the bone appears to be well vascularized, possibly as a result of weight-bearing and bending during hopping (Alexander and Vernon 1975). The kangaroo fibula provides points of attachment for the *M. extensor digitorum longus*, *M. extensor digitorum lateralis*, *M. peroneus digiti IV*, *M. peroneus longus*, *M. peroneus digiti V, M. flexor digitorum profundus,* and *M. popliteus* muscles, largely associated with flexing, extending and abducting the digits (Hopwood and Butterfield, 1990). Its principal role during saltorial locomotion involves lateral articulations with the main loadbearing femorotibial articulation, with a fibular meniscus and a complex of ligaments, tissues, and muscles restricting movement of the proximal fibula in order to protect against external rotation of the tibia (Miller et al. 2017). Therefore, the kangaroo fibula stabilizing the kangaroo ankle is well vascularized.

Intra-skeletal trends in vascular canal density

There appears to be a 'tiered' vascular canal density in the long bones, with the larger limb bones – the humerus and the femur – being least densely vascular, followed by the smaller limb bones – the radius, ulna and tibia, with the one exception of the fibula. Although kangaroos are mostly known for their bipedal gait, they use pentapedal locomotion more frequently than hopping (O'Connor et al. 2014; Windsor and Dagg 1971). This form of locomotion, where the forefeet and tail are the main load-bearing elements when the hind feet are lifted, would result in greater mechanical loading on the femur and humerus, relative to the tibia, ulna and radius. This is observed in our sample through the 'tiers' of vascularity. From this perspective, a direct biomechanical comparison of lower to upper limb biomechanical environments to humans cannot be ascertained, but our results provide an insight into vascularity of the long bones in this one kangaroo individual.

Our results would explain why in studies of human long bones lower cortical porosity is seen in slender bones where remodeling is suppressed, yet more active remodeling noted in more robust bones (e.g. Goldman et al. 2014). In humans, there is likely to be large intra-specific variation in behaviors that would underlie remodeling experienced at the leg, and thus scaling relationships seen between robusticity and the underlying microstructure (Miszkiewicz and Mahoney 2019). Indeed, a larger range of motion in the arms than legs might also introduce more biomechanical load in the ulna and radius compared to the fibula, which has been found to be generally less susceptible to biomechanical load unless under constant medio-lateral movements in humans (Marchi and Shaw 2011). However, lower limbs in humans regularly receive compression from bipedal movements, whereas a kangaroo's locomotion is supported by the tail, offsetting and re-distributing the load experienced by the hindlimb (Alexander and Vernon 1975). Here, the positive relationship between radius and thoracic rib vascular density and the Ct.Wi.RI, but negative relationship with the tibia, still indicates some extent of biomechanical load accommodation in the robust tibia. In humans, it is one of the main weight-bearing bones and has been observed as more robust under increased strains such as those found in professional athletes (Auerbach et al. 2017; Shaw and Stock 2009).

The pioneering work by Schaffler and Burr (1984) examining intra-skeletal bone remodeling in primates indicated relationships between remodeled bone and habitual loading such that bipeds tend to show the highest proportion of osteonal bone in their lower limbs. Their study, however, considered secondary osteons only, and examined full cross-sections, which is different from the methods employed in our study. Our results support this theory in differences between weight-bearing versus non-weight-bearing bones, such as the widely studied femur versus rib. Cho and Stout (2011) identified higher osteon population density (OPD) and remodeling rates in the human rib than femur, which although uses OPD, could suggest that vascular density would be higher in the human rib compared to the human femur, similar to our results. In contrast, Pfeiffer et al. (2006) found no relationship between secondary osteon area and biomechanical load or metabolic activity patterns in the human femur or rib; however they did identify increased secondary osteon area in the rib when compared to the femur. However, when discussing bone biomechanical effects, it is necessary to treat OPD measures cautiously given that it is a poor predictor of habitual loading. While secondary osteon area provides different data to vascular density, it suggests further investigation similar to ours is necessary in human samples.

Despite differences in the variables examined, human studies do suggest that the femur experiences significantly more loading effects through weight-bearing, and more irregular loading cycles than that of the rib, which our results here appear to agree with (Cho and Stout 2011; Pfeiffer et al. 2006).

LIMITATIONS

We opted here to account for bone size and morphology differences with the use of robusticity indices for ease of histological analysis instead of scaling ROI size to a percentage of the cross-section for each individual bone. Future research should undertake either this scaling of ROI size for each bone, or the assessment of an entire cross-section taking into account bone tissue types present throughout each cross-section. Because we only focused on longitudinal canals, we also suggest future examination of vessel orientation and connectivity (e.g. Britz et al. 2012). Kangaroos are marsupials whose forelimb developmental pathway differs from that of humans as joeys need forelimb strength early in ontogeny to be able to climb out of the mother's pouch (Cooper and Steppan 2010). This highlights caution when translating our results to other animal models as bones of different functions have related mechanical and mineralization properties (Currey et al. 1979). Thus, ideally, future kangaroo bone histology research should also take into consideration measures such as bone mineral density. Finally, the kangaroo examined here was of unknown age and sex, yet sexual dimorphism and ontogenetic processes are relevant to bone robusticity measures and underlying bone physiology (Warburton et al. 2013; Chinsamy and Warburton, 2021), so sexed kangaroos should also be included in future assessments.

CONCLUSION

We use a kangaroo case study to demonstrate that the thoracic rib, and potentially the fibula, are the preferred bones for investigations of metabolic influence on bone microstructure. This is the first report of kangaroo bone vessel densities across a series of major bones of the skeleton. Kangaroos share several biomechanical demands with humans due to their use of bipedal locomotion (Fatima et al. 2019) and could thus provide a useful skeletal model for studying metabolic influence on bone microstructure in the future.

ACKNOWLEDGMENTS

Stewart receives PhD funding through an Australian Government Research Training Program (AGRTP) Scholarship. Louys (FT160100450) and Miszkiewicz (DE190100068) receive funding from the Australian Research Council (ARC). David McGregor (ANU) and Jambhika Godara (Olympus Australia) offered technical assistance. Microscopy equipment at the ANU is funded by the ARC and ANU College of Arts and Social Sciences. We are indebted to the reviewers for their constructive feedback on this study.

REFERENCES

Agnew AM, Stout SD (2012) Brief communication: Reevaluating osteoporosis in human ribs: The role of intracortical porosity. Am J Phys 148:462–466

Alexander RM, Vernon A (1975). The mechanics of hopping by kangaroos (Macropodidae). J Zool 177:265–303

Auerbach BM, Gooding AF, Shaw CN, Sylvester AD (2017) The relative position of the human fibula to the tibia influences cross-sectional properties of the tibia. Am J Phys 163:148–157

Britz HM, Jokihaara J, Leppänen OV, Järvinen TL, Cooper DM (2012) The effects of immobilization on vascular canal orientation in rat cortical bone. J Anat 220:67–76

Celik M, Cascini M, Haouchar D et al. (2019) A molecular and morphometric assessment of the systematics of the *Macropus* complex clarifies the tempo and mode of kangaroo evolution. Zool J Linn Soc 186:793–812

Chinsamy A, Warburton NM (2021) Ontogenetic growth and the development of a unique fibrocartilage entheses in *Macropus fuliginosus*. Zool 144: 125860.

Cho H, Stout SD (2011) Age-associated bone loss and intraskeletal variability in the Imperial Romans. J Anthropol Sci 89:109–125

Cooper WJ, Steppan SJ (2010) Developmental constraint on the evolution of marsupial forelimb morphology. Aust J Zool 58:1–15

Cooper DM, Turinsky AL, Sensen CW, Hallgrímsson B (2003) Quantitative 3D analysis of the canal network in cortical bone by micro-computed tomography. Anat Rec 274:169–179

Cooper DML, Kawalilak CE, Harrison K, Johnston BD, Johnston JD (2016) Cortical bone porosity: what is it, why is it important, and how can we detect it? Curr Osteoporos Rep 14:187–198

384 Coulson G, Eldridge M (2010) Macropods: the biology of kangaroos, wallabies, and rat-kangaroos. CSIRO
385 Publishing, Australia

386 Cox G, Sealy J (1997) Investigating identity and life histories: isotopic analysis and historical documentation
387 of slave skeletons found on the Cape Town foreshore, South Africa. Int J Hist Archaeol 1:207–224

388 Croker SL, Reed W, Donlon D (2016) Comparative cortical bone thickness between the long bones of humans
389 and five common non-human mammal taxa. Forensic Sci Int 260:104.e1–104.e17

390 Crowder C, Rosella L (2007) Assessment of intra- and intercostal variation in rib histomorphometry: Its impact
391 on evidentiary examination. J Forensic Sci 52:271–276

392 Currey JD (1979) Mechanical properties of bone tissues with greatly differing functions. J Biomech 12:313–
393 319

394 Dawson TJ (1995) Kangaroos: biology of the largest marsupials. Cornell University Press, New York

395 Dawson R, Milne N, Warburton NM (2014) Muscular anatomy of the tail of the western grey kangaroo,
396 Macropus fuliginosus. Aust J Zool 62:166–174

397 Dawson RS, Warburton NM, Richards HL, Milne N (2015) Walking on five legs: investigating tail use during
398 slow gait in kangaroos and wallabies. Aust J Zool 63:192–200

399 Dempster DW, Compston JE, Drezner MK et al. (2013) Standardized nomenclature, symbols, and units for
400 bone histomorphometry: a 2012 update of the report of the ASBMR Histomorphometry Nomenclature
401 Committee. J Bone Miner Res 28: 2–17

402 Dominguez VM, Agnew AM (2016) Examination of factors potentially influencing osteon size in the human
403 rib. Anat Rec 299:313–324

404 Eleazer CD, Jankauskas R (2016) Mechanical and metabolic interactions in cortical bone development. Am J
405 Phys Anthropol 160:317–333
406

Elissamburu A, Vizcaíno SF (2004) Limb proportions and adaptations in caviomorph rodents (Rodentia: Caviomorpha). J Zool 262:145–159

Fahy GE, Deter C, Pitfield R, Miszkiewicz JJ, Mahoney P (2017) Bone deep: variation in stable isotope ratios and histomorphometric measurements of bone remodelling within adult humans. J Archaeol Sci 87:10–16

Fatima M, Scholes CJ, Zhong E, Kohan L (2019) Towards a dynamic model of the kangaroo knee for clinical insights into human knee pathology and treatment: Establishing a static biomechanical profile. Biomimetics 4:52

Flannery TF (1982) Hindlimb structure and evolution in the kangaroos (Marsupialia: Macropodoidea). In: Rich PV, Thompson EM (eds) The Fossil Vertebrate Record of Australia. Monash University Press, Melbourne, pp 508–524

Francillon-Vieillot H, de Buffrénil V, Castanet JD et al. (1990) Microstructure and mineralization of vertebrate skeletal tissues. In: Carter JG (ed) Skeletal Biomineralization: Patterns, Processes and Evolutionary Trends, Vol.1. Van Nostrand Reinhold, New York, pp 471–530

Frost HM (1964) The Laws of Bone Structure. CC Thomas, Michigan.

Frost HM (1969) Tetracycline-based histological analysis of bone remodeling. Calcif Tissue Int 3: 211–237

Frost HM (2000) The Utah paradigm of skeletal physiology: an overview of its insights for bone, cartilage and collagenous tissue organs. J Bone Miner Metab 18:305–316

Goh JC, Mech AM, Lee EH, Ang EJ, Bayon P, Pho RW (1992) Biomechanical study on the load-bearing characteristics of the fibula and the effects of fibular resection. Clin Ortho Relat Res 279:223–8

Goldman HM, Hampson NA, Guth JJ, Lin D, Jepsen KJ (2014) Intracortical remodeling parameters are associated with measures of bone robustness. Anat Rec 297:1817–1828

429 Hart NH, Nimphius S, Rantalainen T, Ireland A, Siafarikas A, Newton RU (2017) Mechanical basis of bone
430 strength: influence of bone material, bone structure and muscle action. J Musculoskelet Neuronal
431 Interact 17:114–139

432 Harvey KJ, Warburton N (2010) Forelimb musculature of kangaroos with particular emphasis on the tammar
433 wallaby Macropus eugenii (Desmarest, 1817). Aust Mammal 32:1–9

434 Hedges RE, Clement JG, Thomas CDL, O'Connell TC (2007) Collagen turnover in the adult femoral mid-shaft:
435 Modeled from anthropogenic radiocarbon tracer measurements. Am J Phys Anthropol 133:808–816

436 Hopwood PR, Butterfield RM (1990) The locomotor apparatus of the crus and pes of the Eastern Gray
437 Kangaroo, *Macropus giganteus*. Aust J Zool 38:397–413

438 Huttenlocker AK, Woodward HN, Hall BK (2013) The biology of bone. In: Padian K, Lamm E-T (eds) Bone
439 histology of fossil tetrapods: advancing methods, analysis, and interpretation. University of California
440 Press, Berkeley, pp 13–34

441 Iwaniec UT, Crenshaw TD, Schoeninger MJ, Stout SD, Ericksen MF (1998) Methods for improving the
442 efficiency of estimating total osteon density in the human anterior mid-diaphyseal femur. Am J Phys
443 107:13–24

444 Kondo T, Matsumoto I, Lanteri CJ, Sly PD (2000) Respiratory mechanics during mechanical ventilation: A
445 model study on the effects of leak around a tracheal tube. Pediatr Pulmonol 24:423–428

446 Lad SE, McGraw WS, Daegling DJ (2019) Haversian remodeling corresponds to load frequency but not strain
447 magnitude in the macaque (*Macaca fascicularis*) skeleton. Bone 127:571–576

448 Lafage-Proust MH, Roche B, Langer M, Cleret D, Bossche AV, Olivier T, Vico L (2015) Assessment of bone
449 vascularization and its role in bone remodeling. Bonekey Rep 4: 662.

450 Lamb AL, Evans JE, Buckley R, Appleby J (2014) Multi-isotope analysis demonstrates significant lifestyle
451 changes in King Richard III. J Archaeol Sci 50:559–565

452 Lieberman DE, Polk JD, Demes B (2004) Predicting long bone loading from cross-sectional geometry. Am J
453 Phys Anthropol 123:156–171

454 Marchi D, Shaw CN (2011) Variation infibular robusticity reflects variation in mobility patterns. J Hum Evol
455 61:609–616

456 Marenzana M, Arnett TR (2013) The key role of the blood supply to bone. Bone Res 1:203–215

457 McGowan CP, Skinner J, Biewener AA (2008) Hind limb scaling of kangaroos and wallabies (superfamily
458 Macropodoidea): implications for hopping performance, safety factor and elastic savings. J Anat
459 212:153–163

460 Mendelow H, Hamilton JB (1950) A new technique for rapid freezing and dehydration of tissues for histology
461 and histochemistry. Anat Rec 107:443–451

462 Miller AC, Cake MA, Warburton NM (2017) The fibular meniscus of the kangaroo as an adaptation against
463 external tibial rotation during saltatorial locomotion. J Anat 231:931–938

464 Miszkiewicz JJ, Mahoney P (2016) Ancient human bone microstructure in Medieval England: Comparisons
465 between two socio-economic groups. Anat Rec 299:42–59

466 Miszkiewicz JJ, Mahoney P (2019) Histomorphometry and cortical robusticity of the adult human femur. J
467 Bone Miner Metab 37:90–104

468 Miszkiewicz JJ, Louys J, O'Connor S (2019) Microanatomical record of cortical bone remodeling and high
469 vascularity in a fossil giant rat midshaft femur. Anat Rec 302:1934–1940

470 Miszkiewicz JJ, Louys J, Beck RM, Mahoney P, Aplin K, O'Connor S (2020) Island rule and bone metabolism
471 in fossil murines from Timor. Biol J Linn Soc 129:570–586

472 Mulhern DM (2000) Rib remodeling dynamics in a skeletal population from Kulubnarti, Nubia. Am J Phys
473 Anthropol 111:519–530

474 Nilsson MA, Churakov G, Sommer M et al. Tracking marsupial evolution using archaic genomic retroposon
475 insertions. PLoS Biol 2010. doi:10.1371/journal.pbio.1000436

476 O'Connor SM, Dawson TJ, Kram R, Donelan JM. The kangaroo's tail propels and powers pentapedal
477 locomotion. Biol Lett 2014. doi:10.1098/rsbl.2014.0381

478 Paine RR, Brenton BP (2006) Dietary health does affect histological age assessment: an evaluation of the Stout
479 and Paine (1992) age estimation equation using secondary osteons from the rib. J Forensic Sci 51:489–
480 492

481 Peterson MC, Riggs MM (2010) A physiologically based mathematical model of integrated calcium
482 homeostasis and bone remodeling. Bone 46(1), 49-63

483 Pfeiffer S, Crowder C, Harrington L, Brown M (2006) Secondary osteon and Haversian canal dimensions as
484 behavioral indicators. Am J Phys Anth 131:460–468

485 Poole WE (1976) Breeding Biology and Current Status of the Grey Kangaroo, *Macropus Fulginosus*
486 *Fulginosus*, of Kangaroo Island, South Australia. Aust J Zool 24:169–187

487 Price GJ, Louys J, Smith GK, Cramb J. Shifting faunal baselines through the Quaternary revealed by cave
488 fossils of eastern Australia. PeerJ 2019. doi:10.7717/peerj.6099

489 Prideaux GJ, Warburton NM (2010) An osteology-based appraisal of the phylogeny and evolution of kangaroos
490 and wallabies (Macropodidae: Marsupialia). Zool J Linn Soc 159:954–987

491 Prisby RD (2017) Mechanical, hormonal and metabolic influences on blood vessels, blood flow and bone. J
492 Endocrinol 235:R77–R100

493 Reed EH (2001) Disarticulation of kangaroo skeletons in semi-arid Australia. Aust J Zool 49:615–632

494 Richardson K (2012) Australia's amazing kangaroos: their conservation, unique biology and coexistence with
495 humans. CSIRO Publishing, Australia.

496 Robling AG, Stout SD (2003) Histomorphology, geometry, and mechanical loading in past populations. In:
497 Agarwal SC, Stout SD (eds) Bone loss and osteoporosis. Springer, Boston, USA, pp 189–20

498 Robling AG, Castillo AB, Turner CH (2006) Biomechanical and molecular regulation of bone remodeling.
499 Annu Rev of Biomed Eng 8:455–498

500 Rubin CT, Lanyon LE (1987) Osteoregulatory nature of mechanical stimuli: function as a determinant for
501 adaptive remodeling in bone. J Orthop Res 5:300–310

502 Russell EM (1974) The biology of kangaroos (Marsupialia-Macropodidae). Mamm Rev 4:1–59

503 Schaffler MB, Burr DB (1984) Primate cortical bone microstructure: relationship to locomotion. Am J Phys
504 Anthropol 65:191–197

505 Shaw CN, Stock JT (2009) Intensity, repetitiveness, and directionality of habitual adolescent mobility patterns
506 influence the tibial diaphysis morphology of athletes. Am J Phys 140:149–159

507 Shea JE, Hallows RK, Ricks S, Bloebaum RD (2002) Microvascularization of the hypermineralized calcified
508 fibrocartilage and cortical bone in the sheep proximal femur. Anat Rec 268:365–370

509 Skedros JG, Knight AN, Clark GC et al. (2013) Scaling of Haversian canal surface area to secondary osteon
510 bone volume in ribs and limb bones. Am J Phys 151:230–244

511 Stewart TJ, Louys J, Miszkiewicz JJ. Evaluating the extent to which rib microstructure reflects its macro-
512 anatomical form. Conference paper presented at the International Symposium on Palaeohistology July
513 31 – August 4 2019, Cape Town, South Africa, p 63

514 Szalay FS (1994) Evolutionary History of the Marsupials and an Analysis of Osteological Characters.
515 Cambridge University Press, New York.

516 Takebe K, Nakagawa A, Minami H, Kanazawa H, Hirohata K (1984) Role of the fibula in weight-bearing. Clin
517 Orthop Relat Res 184:289–292

518 Taylor R (1990) Interpretation of the correlation coefficient: a basic review. J Diagn Med Sonogr 6(1), 35-39.

519 Tommerup LJ, Raab DM, Crenshaw TD, Everett LS (1993) Does weight-bearing exercise affect non-weight-
520 bearing bone? J Bone Miner Res 8:1053–1058

521 Vajda EG, Bloebaum RD (1999) Age-related hypermineralization in the female proximal human femur. Anat
522 Rec 255:202–211

523 Villa C, Lynnerup N (2010) Technical note: A stereological analysis of the cross-sectional variability of the
524 femoral osteon population. Am J Phys 142:491–496

525 Viboolvorakul S, Niimi H, Wongeak-in N, Eksakulkla S, Patumraj S (2009) Increased capillary vascularity in
526 the femur of aged rats by exercise training. Microvasc Res 78:459–463

527 Vizcaíno SF, Milne N (2002) Structure and function in armadillo limbs (Mammalia: Xenarthra: Dasypodidae).
528 J Zool 257:117–127

529 Walker MM, Louys J, Herries AI, Price GJ, Miszkiewicz JJ. Humerus midshaft histology in a modern and fossil
530 wombat. Aust Mamm 2020. doi:10.1071/AM20005

531 Warburton NM, Bateman PW, Fleming PA (2013) Sexual selection on forelimb muscles of western grey
532 kangaroos (Skippy was clearly a female). Biol J Linn Soc 109:923–931

533 Williams D (1994) Guide to cleaner technologies: cleaning and degreasing process changes. DIANE
534 Publishing, Washington, USA

535 Windsor DE, Dagg AI (1971) The gaits of the Macropodinae (Marsupialia). J Zool 163:165–175

536 Wu PH, Gibbons M, Foreman SC et al. (2019) Cortical bone vessel identification and quantification on contrast-
537 enhanced MR images. Quant Imag Med Surg 9:928–941

538 van Der Meulen MC, Beaupre GS, Carter DR (1993) Mechanobiologic influences in long bone cross-sectional
539 growth. Bone 14(4), 635-642

540 Ziv V, Wagner HD, Weiner S (1996) Microstructure-microhardness relations in parallel-fibered and lamellar
541 bone. Bone 18:417–428

Figure 1: Kangaroo specimen bones from the right side prior to sectioning at midshaft (red dashed line). Note the tibia and the fibula are composite images stitched from two images. Biomechanical environments for bone group are outlined. Scale bars (black lines to the bottom of the image underneath each bone) are all 5 cm. The humerus, radius, ulna, femur, and ribs (superior during a bipedal stance) are shown from the anterior/cranial view. The tibia and fibula are shown from the medial view.

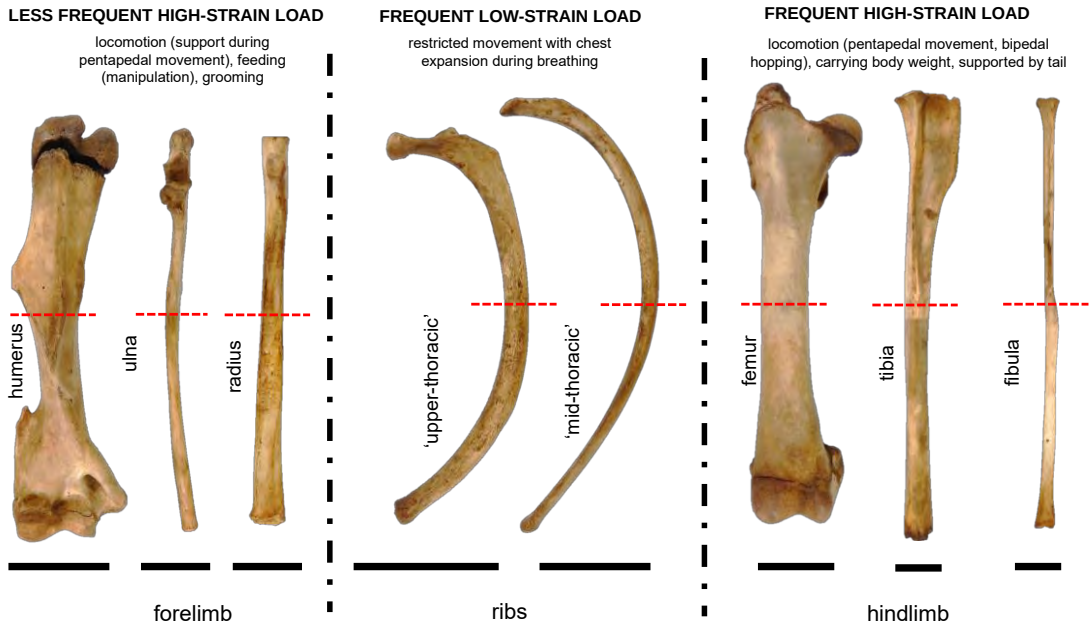

549 **Figure 2**: (a) Cross-sections of bones for morphological comparison. (b) Sample histological image showing

550 an example of a longitudinal vessel (red circle) in a region of the thoracic rib.

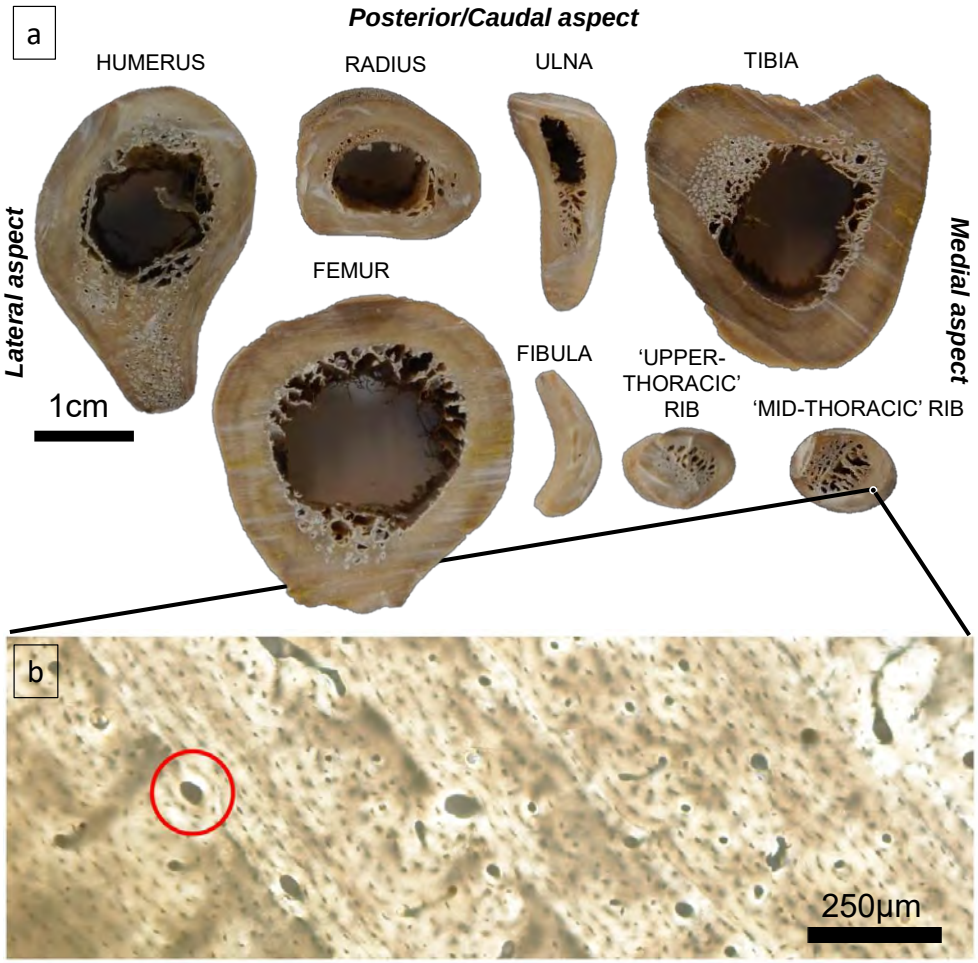

551

552

Figure 3: (a) Femur cross-section with crosshairs and ROIs overlaid - three per anatomical aspect (anterior/cranial, posterior/caudal, medial, lateral). (b) Posterior femur section with three 1mm^2 ROIs delineated. (c) An example of bone histology seen in one of the ROIs, where white ticks indicate vessels we would consider countable. Red crosses indicate vessels not countable (e.g. due to being cut off by the image border).

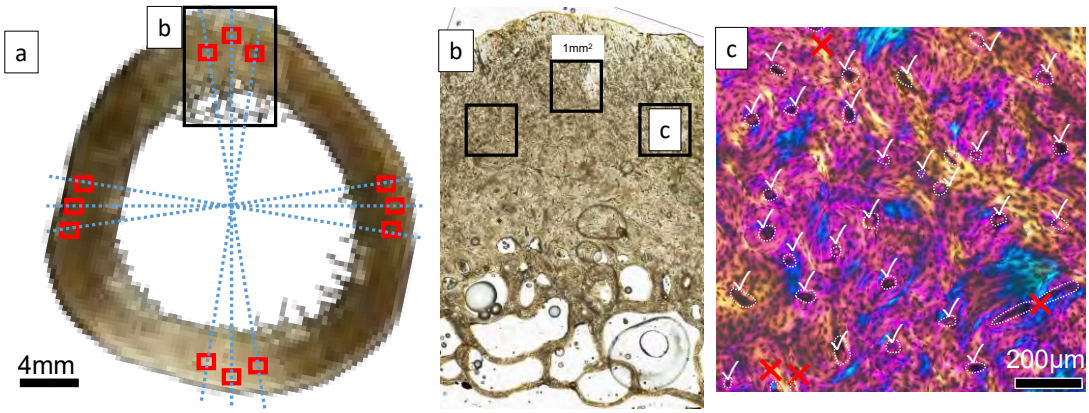

Figure 4: An example of longitudinal vessels counted in this study in a region of posterior/caudal sub-periosteal femur bone (taken using lambda compensated polarized light) in our kangaroo specimen showing simple primary vessel (SPV), Haversian canal within a secondary osteon (HC within SO), and a simple vessel with a primary osteon (SV within PO).

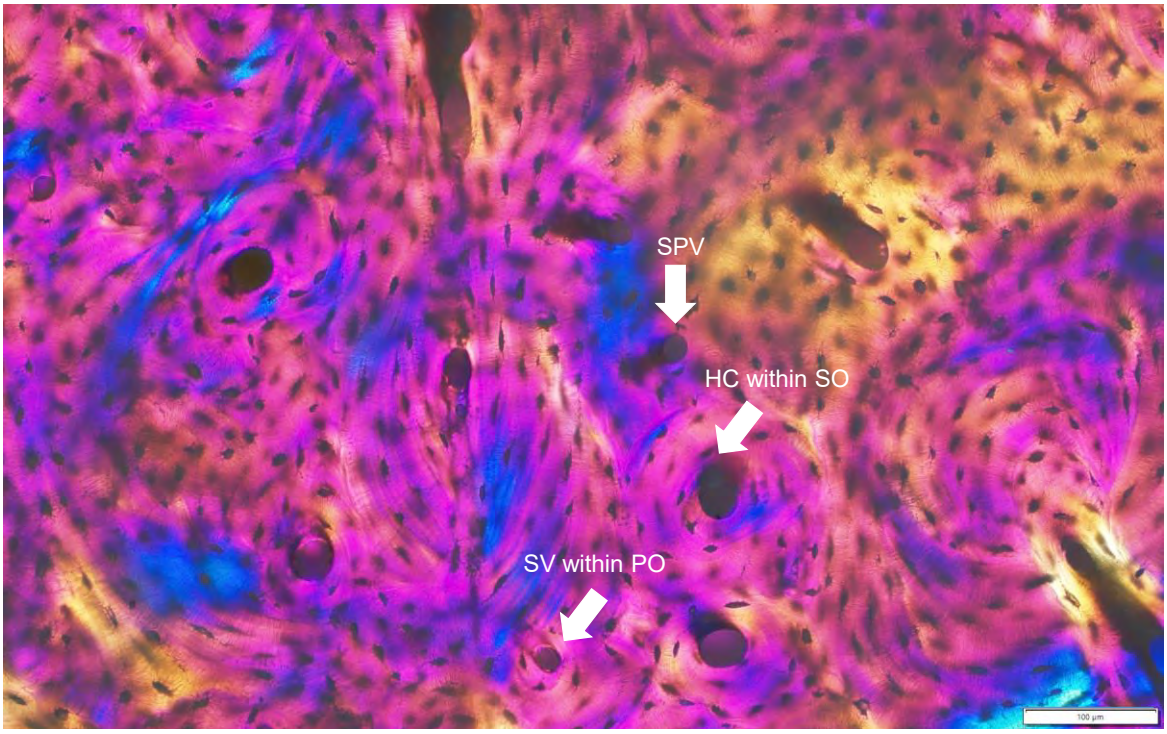

Figure 5: Graphical summary of our findings. (a) Raw vascular canal density per bone prior to correcting by robusticity indices. (b) Vascular canal density corrected by midshaft circumference (unitless). (c) Vascular canal density corrected by cortical width (unitless). (d) Scattergram of corrected total vascular canal density by midshaft circumference robusticity index. Note: total vascular canal density was used in this case because each bone only had one midshaft circumference value, and twelve vascular canal density values (one for each ROI), which cannot be correlated in a statistically competent way. (e) Scattergram of corrected vascular canal density by cortical width robusticity index. Note: Here we used corrected vascular canal density values as each ROI datapoint had corresponding vascular canal density and cortical width values. (f) Friedman's pairwise comparison shows differences in vascular canal density between individual bones. Black lines indicate statistically significant differences between vascular canal density values. Note: Units of measurements are provided where possible on each diagram in this figure. Where units of measurement are not included, values are indexed, meaning they are composite statistics, which summarize and rank specific observations.

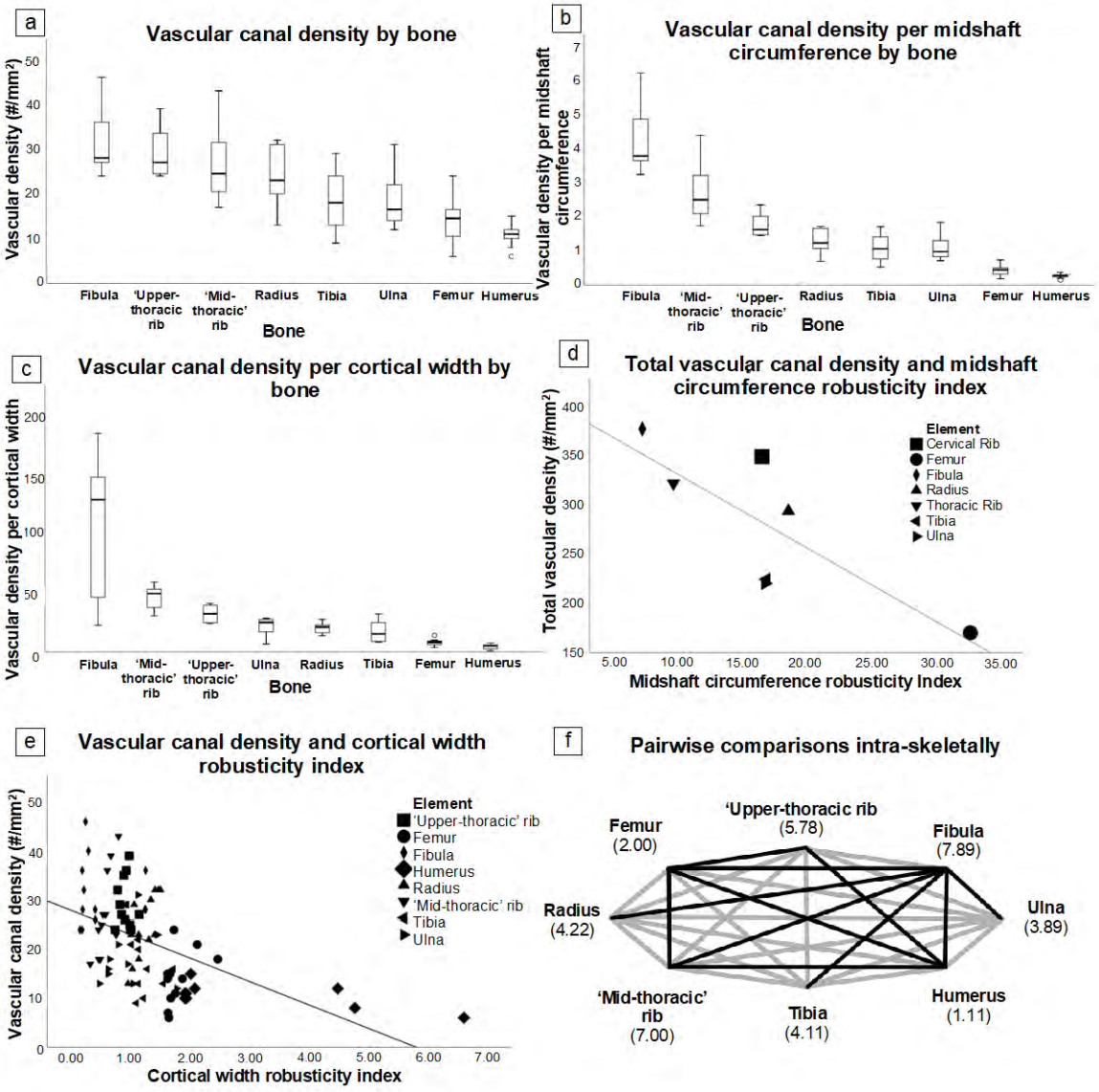
a
Vascular canal density by bone
Vascular density (#/mm²)
Fibula
'Upper-thoracic rib
'Mid-thoracic' rib
Radius
Tibia
Ulna
Femur
Humerus
Bone
b
Vascular canal density per midshaft circumference by bone
Vascular density per midshaft circumference
Bone
c
Vascular canal density per cortical width by bone
Vascular density per cortical width
d
Total vascular canal density and midshaft circumference robusticity index
Total vascular density (#/mm²)
Element
Cervical Rib
Femur
Fibula
Radius
Thoracic Rib
Tibia
Ulna
Midshaft circumference robusticity Index
e
Vascular canal density and cortical width robusticity index
Vascular canal density (#/mm²)
Element
'Upper-thoracic' rib
Femur
Fibula
Humerus
Radius
'Mid-thoracic' rib
Tibia
Ulna
Cortical width robusticity index
f
Pairwise comparisons intra-skeletally
'Upper-thoracic rib (5.78)
Femur (2.00)
Fibula (7.89)
Radius (4.22)
Ulna (3.89)
'Mid-thoracic' rib (7.00)
Tibia (4.11)
Humerus (1.11)

578

579 **Table 1**: Equations and definitions for vascular density and robusticity indices accounting for cortical thickness

580 and midshaft circumference.

Variable (abbreviation)	Definition (and equation if applicable)
Maximum length in mm (Max.Length)	Measured along the bone long axis, which was straight for the limb bones. Rib maximum length was measured along its curvature. (e.g. Croker et al., 2016).
Midshaft circumference (Circ)	The circumference of the bone shaft measured at the midpoint of the maximum length. (e.g. Stock and Shaw 2007; Miszkiewicz and Mahoney, 2016).
Cortical width (Ct.Wi)	Measured from the innermost endosteal perimeter to the outermost periosteal surface (e.g. Vajda and Bloebaum 1999). This was recorded from cross-section images using ImageJ vol. 1.52 ("straight line" tool) at the outer axis of each ROI for each bone (Fig. 3a).
Vascular canal density (Ca.Dn)	This was the number of longitudinal vessels per mm^2. These were counted if they were rounded, complete and were wholly captured within the ROI. Those that were cut off by the ROI image border were not counted. (e.g. Wu et al., 2019; Shea et al., 2002).
Total vascular density (Tt.Ca.Dn)	As Ca.Dn above, except this was the summed number of counted vessels per mm^2 per bone type. As there were a maximum of 12 ROIs for each bone, this meant the total vessel count was per $12mm^2$. The humerus was excluded from portions of the analysis that included this measure as it only had 9 ROIs available for examination.
Cortical width robusticity index (Ct.Wi.RI)	This refers to how gracile/slender or robust bone is as deduced from its shaft size in relation to maximum length: (cortical width / maximum length) x 100. (e.g. Stock and Shaw 2007; Miszkiewicz and Mahoney, 2016; e.g. Elissamburu & Vizcaino, 2004; Vizcaíno and Milne, 2002).
Midshaft circumference robusticity index (Circ.RI)	As above, except this uses midshaft circumference as a measure of midshaft 'size': (midshaft circumference / maximum length) x 100. (e.g. Stock and Shaw 2007; Miszkiewicz and Mahoney, 2016; e.g. Elissamburu & Vizcaino, 2004; Vizcaíno and Milne, 2002).
Vascular canal density per cortical width robusticity index (Ca.Dn/Ct.Wi.RI)	This value represents a bone vascular canal density corrected by bone robusticity index derived from cortical width and total bone length: vascular canal density/ cortical width robusticity index (e.g. Miszkiewicz et al., 2020).
Vascular canal density per midshaft circumference robusticity index (Ca.Dn/Circ.Ri)	As above, except this value uses bone robusticity index derived from midshaft circumference and bone length: vascular density / midshaft circumference robusticity: vascular canal density/ midshaft circumference robusticity index. (e.g. Miszkiewicz et al., 2020).

581

582

583 **Table 2**: Descriptive statistics summarizing the bone morphological and histological data. Min.: minimum,
584 Max.: maximum, SD: standard deviation, n/a: not applicable. See Table 1 for definitions of abbreviated
585 variables.

Bone	Histological or macroscopic variable	Min.	Max.	Mean/ value	SD
'Upper-thoracic' rib (n = 1, ROI n = 12)	Ca.Dn (#/mm^2)	24.00	39.00	29.00	5.24
	Ct.Wi (mm)	1.40	2.16	1.74	0.21
	Ct.Wi.RI	0.75	1.15	0.93	0.11
	Ca.Dn/Ct.Wi.RI	23.41	40.41	31.67	6.72
	Ca.Dn/Circ.Ri	1.45	2.35	1.75	0.32
	Max.Length (mm)	n/a	n/a	187.00	n/a
	Circ (mm)	n/a	n/a	31.00	n/a
	Circ.RI	n/a	n/a	16.58	n/a
Femur (n = 1, ROI n = 12)	Ca.Dn (#/ mm^2)	6.00	24.00	14.17	5.27
	Ct.Wi (mm)	4.47	6.78	4.92	0.71
	Ct.Wi.RI	1.63	2.47	1.79	0.26
	Ca.Dn/Ct.Wi.RI	3.63	13.83	7.87	2.74
	Ca.Dn/Circ.Ri	0.18	0.74	0.43	0.16
	Max.Length (mm)	n/a	n/a	274.50	n/a
	Circ (mm)	n/a	n/a	89.50	n/a
	Circ.RI	n/a	n/a	32.60	n/a
Fibula (n = 1, ROI n = 12)	Ca.Dn (#/ mm^2)	24.00	46.00	31.33	6.84
	Ct.Wi (mm)	0.76	5.98	2.43	2.16
	Ct.Wi.RI	0.16	1.26	0.51	0.46
	Ca.Dn/Ct.Wi.RI	22.19	181.34	103.55	59.86
	Ca.Dn/Circ.Ri	3.25	6.23	4.24	0.93
	Max.Length (mm)	n/a	n/a	474.00	n/a
	Circ (mm)	n/a	n/a	35.00	n/a
	Circ.RI	n/a	n/a	7.38	n/a
Humerus (n = 1, ROI n = 9)	Ca.Dn (#/ mm^2)	6.00	15.00	10.56	2.55
	Ct.Wi (mm)	3.87	13.29	6.20	3.53
	Ct.Wi.RI	1.92	6.59	3.07	1.75
	Ca.Dn/Ct.Wi.RI	0.91	7.43	4.47	2.18
	Ca.Dn/Circ.Ri	0.15	0.37	0.26	0.06
	Max.Length (mm)	n/a	n/a	201.50	n/a
	Circ (mm)	n/a	n/a	81.50	n/a
	Circ.RI	n/a	n/a	40.45	n/a
Radius (n = 1, ROI n = 12)	Ca.Dn (#/ mm^2)	13.00	32.00	24.42	6.60
	Ct.Wi (mm)	2.52	3.93	3.23	0.51
	Ct.Wi.RI	0.97	1.51	1.24	0.19
	Ca.Dn/Ct.Wi.RI	13.43	27.11	19.58	4.03
	Ca.Dn/Circ.Ri	0.70	1.71	1.31	0.35
	Max.Length (mm)	n/a	n/a	260.50	n/a
	Circ (mm)	n/a	n/a	48.50	n/a
	Circ.RI	n/a	n/a	18.62	n/a
'Mid-thoracic' rib (n = 1, n ROI = 12)	Ca.Dn (#/ mm^2)	17.00	43.00	26.75	8.42
	Ct.Wi (mm)	0.89	2.15	1.56	0.37
	Ct.Wi.RI	0.33	0.81	0.59	0.14
	Ca.Dn/Ct.Wi.RI	29.98	58.11	45.81	9.48
	Ca.Dn/Circ.Ri	1.74	4.40	2.74	0.86
	Max.Length (mm)	n/a	n/a	266.00	n/a
	Circ (mm)	n/a	n/a	26.00	n/a
	Circ.RI	n/a	n/a	9.77	n/a
Tibia (n = 1, n ROI = 12)	Ca.Dn (#/ mm^2)	9.00	29.00	18.67	6.96
	Ct.Wi (mm)	4.40	8.29	5.66	1.20
	Rbty.Ct.Wi	0.91	1.72	1.18	0.25
	Ca.Dn/Ct.Wi.RI	8.15	31.60	17.17	9.01
	Ca.Dn/Circ.Ri	0.53	1.71	1.10	0.411
	Max.Length (mm)	n/a	n/a	481.50	n/a
	Circ (mm)	n/a	n/a	81.50	n/a
	Circ.RI	n/a	n/a	16.93	n/a
Ulna (n = 1, n ROI = 12)	Ca.Dn (#/ mm^2)	12.00	31.00	18.33	5.84
	Ct.Wi (mm)	1.45	5.30	2.77	1.14
	Ct.Wi.RI	0.49	1.78	0.93	0.38
	Ca.Dn/Ct.Wi.RI	6.73	27.99	21.69	6.93

586

587

588 **Table 3**: Results from the Spearman's *Rho* analysis correlating total bone vascularity data (Tt.Ca.Dn) with
589 cortical width (Ct.Wi) and midshaft circumference (Circ) robusticity indices (RIs). *$p < 0.05$, ** $p < 0.01$.

Corrected Ca.Dn correlated with Ct.Wi.RI		
BONE	***Rho***	***p***
'Upper-thoracic' rib	-0.198	0.538
Femur	0.367	0.241
Fibula	0.182	0.571
Humerus	-0.245	0.526
Radius	0.773	0.003**
'Mid-thoracic' rib	0.633	0.027*
Tibia	-0.636	0.026*
Ulna	0.225	0.483

590